

INSPECTING COMPOSITE CERAMIC ARMOR USING ADVANCED SIGNAL PROCESSING TOGETHER WITH PHASED ARRAY ULTRASOUND

J. S. Steckenrider
Illinois College
Jacksonville, IL

W. A. Ellingson and E.R. Koehl
Argonne National Laboratory
Argonne, Illinois USA

T.J. Meitzler
US Army, TARDEC
Warren, MI

ABSTRACT

A series of 16-inch square by 2-inch thick, multi-layered ceramic composite armor specimens have been inspected using a 128 element, 10MHz immersion phased array ultrasound system. Some of these specimens had intentional design defects inserted interior to the specimens. Because of the very large changes in acoustic velocities of the various layered materials, ultrasonic wave propagation is problematic. Further, since the materials used in the layers were stacked such that a lower elastic modulus material was on one side and a higher elastic modulus material was on the other, the side selected for ultrasonic insonification became a significant parameter. To overcome some aspects of the issues with the acoustic wave propagation, two digital signal processing methods were employed. These were: 1)- use of fast Fourier transforms (FFT) and 2)-an integrated signal analysis. Each method has strengths and weaknesses with application in part dependent upon the side of sample used for insonification. The results clearly show that use of these methods significantly improves defect detection. This paper presents the details of the samples used, the issues with ultrasonic wave propagation, a discussion of the two digital signal processing algorithms and results obtained.

INTRODUCTION

Ceramic armor for vehicles offers significant potential improvement over historical materials as it provides a greater capacity for energy absorption and dissipation per unit mass, achieved through very high fracture toughness. However, unlike their metallic predecessors, ceramic materials are much more vulnerable to manufacturing defects, as any such flaws can dramatically reduce that high toughness, thereby compromising the armor's ability to protect military personnel. Thus, an efficient non-destructive evaluation (NDE) method which can identify these defects before the armor is placed into service is critical to their effectiveness¹. Conventional ultrasonic techniques have been used to both locate and characterize such defects in the monolithic ceramic tiles that make up the "backbone" of these armor panels^{2,3}. Furthermore, phased-array ultrasound⁴ (PA-UT) has demonstrated significant improvement over these methods⁵ as it offers both enhanced sensitivity and markedly improved throughput^{6,7}.

Report Documentation Page

Form Approved
OMB No. 0704-0188

Public reporting burden for the collection of information is estimated to average 1 hour per response, including the time for reviewing instructions, searching existing data sources, gathering and maintaining the data needed, and completing and reviewing the collection of information. Send comments regarding this burden estimate or any other aspect of this collection of information, including suggestions for reducing this burden, to Washington Headquarters Services, Directorate for Information Operations and Reports, 1215 Jefferson Davis Highway, Suite 1204, Arlington VA 22202-4302. Respondents should be aware that notwithstanding any other provision of law, no person shall be subject to a penalty for failing to comply with a collection of information if it does not display a currently valid OMB control number.

1. REPORT DATE 08 JAN 2010	2. REPORT TYPE N/A	3. DATES COVERED -			
4. TITLE AND SUBTITLE Inspecting Composite Ceramic Armor Using Advanced Signal Processing Together With Phased Array Ultrasound		5a. CONTRACT NUMBER			
		5b. GRANT NUMBER			
		5c. PROGRAM ELEMENT NUMBER			
6. AUTHOR(S) J. S. Steckenrider; W. A. Ellingson; E.R. Koehl; T.J. Meitzler		5d. PROJECT NUMBER			
		5e. TASK NUMBER			
		5f. WORK UNIT NUMBER			
7. PERFORMING ORGANIZATION NAME(S) AND ADDRESS(ES) Illinois College Jacksonville, IL, USA Argonne National Laboratory Argonne, Illinois USA US Army RDECOM-TARDEC 6501 E 11 Mile Rd Warren, MI 48397-5000, USA		8. PERFORMING ORGANIZATION REPORT NUMBER 20480			
		10. SPONSOR/MONITOR'S ACRONYM(S) TACOM/TARDEC			
9. SPONSORING/MONITORING AGENCY NAME(S) AND ADDRESS(ES)		11. SPONSOR/MONITOR'S REPORT NUMBER(S) 20480			
		12. DISTRIBUTION/AVAILABILITY STATEMENT Approved for public release, distribution unlimited			
13. SUPPLEMENTARY NOTES Presented at 34th International Conference and Exposition on Advanced Ceramics and Composites (ICACC), 24-29 January 2010, Daytona Beach, FL, USA, The original document contains color images.					
14. ABSTRACT					
15. SUBJECT TERMS					
16. SECURITY CLASSIFICATION OF:			17. LIMITATION OF ABSTRACT SAR	18. NUMBER OF PAGES 11	19a. NAME OF RESPONSIBLE PERSON
a. REPORT unclassified	b. ABSTRACT unclassified	c. THIS PAGE unclassified			

While PA-UT has clearly demonstrated its superior performance with regard to the monolithic tiles themselves, actual implementation of ceramic armor incorporates these monolithic tiles into a thick, multi-layered ceramic composite structure. This creates an additional manufacturing step during which additional defects may be introduced, and thus an additional NDE screening would be required to reduce ballistic performance failures caused by these new defects. However, because of the composite nature of the armor panels, the same NDE methodologies used for the monolithic tiles cannot simply be re-applied, as the composite design brings with it additional challenges that must be addressed in order to validate the integrity of the panels.

APPROACH

Figure 1a shows a schematic diagram of the layered structure of the composite armor panels. As shown, there are four primary constituent materials used in the panel makeup: the high-toughness ceramic tiles, a carbon-based matrix used to encase these tiles, an elastomeric layer used to distribute and attenuate mechanical stresses transmitted by the ballistic impact, and a glassy layer which provides a monolithic substrate to support the composite armor. The individual tiles are then arranged side-by-side to form a panel, as shown in Figure 1b where a regular hexagonal tessellation (as was used in this work) is shown.

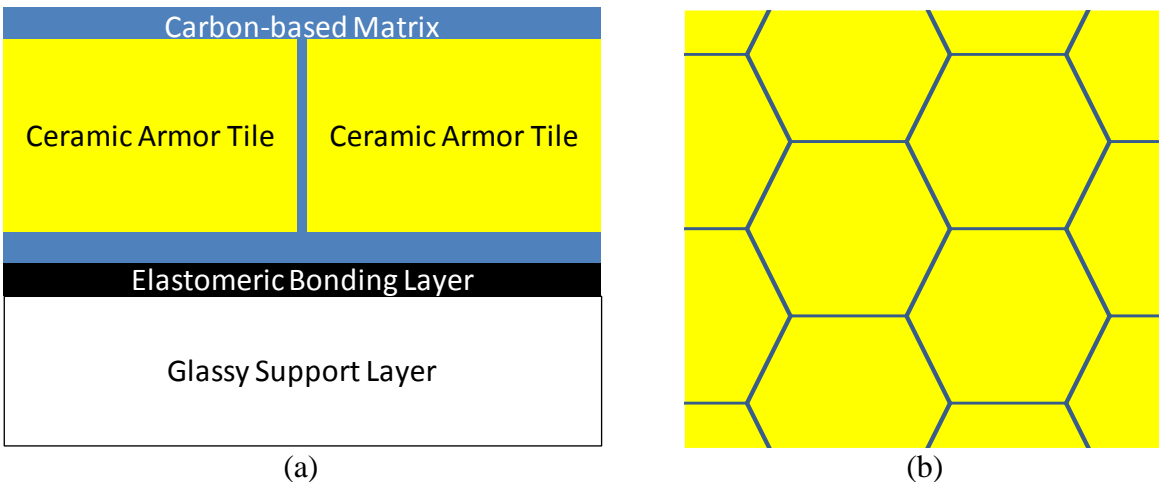


Figure 1. Schematic diagram of composite layered armor panel: a) cross-section and b) top view.

For the test panels investigated in this effort, two modifications were made to the as-designed panel layout. First, planar inclusions were intentionally inserted at the two most critical boundaries (i.e., on either side of the elastomeric bonding layer) to simulate a “disbond” at the locations where it would have the greatest effect in reducing the ballistic performance of the panel. Second, two different armor tiles were used, each made from a different material, so as to reduce the manufacturing investment in each panel. The more resource-intensive material (which also has the greater fracture toughness) was used in the tiles immediately adjacent to the inclusion, while all other tiles were made from the alternate material. Two different configurations for the included “disbond” were used: one in the center of a tile and one at the intersection of three tiles, as shown in Figure 2. Finally, three different “disbond” sizes were used.

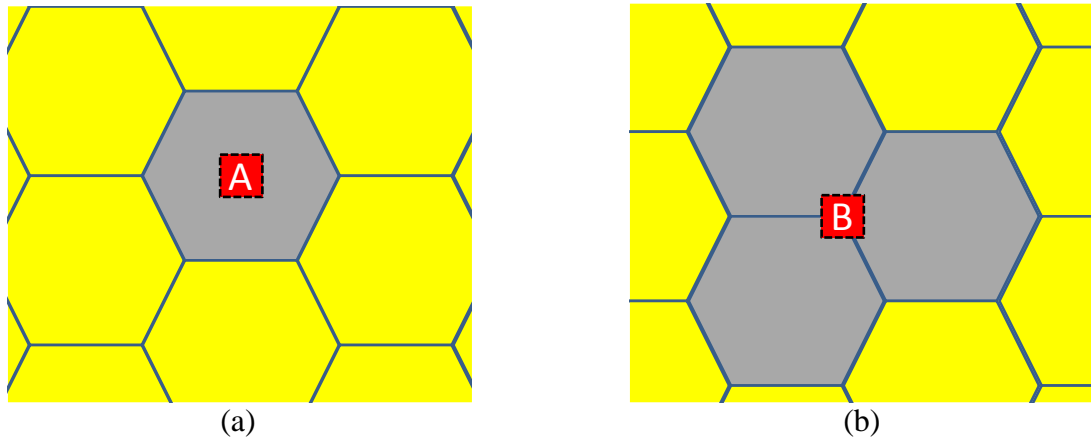


Figure 2. Schematic diagram of composite layered armor panel showing pattern of ceramic tiles (where the darker tile is made from the more resource-intensive material) and location of intentional defects for a) single-tile location and b) tile intersection location.

To evaluate the integrity of these elastomer boundaries the panels were inspected using a water-immersion phased-array system. The phased-array probe consisted of 128 transducer elements operating at 10 MHz with an active area of 64mm by 7 mm. By using a phased-array system we were able to dramatically improve inspection time (by eliminating most of the motion in the scan axis, replacing it with the much faster electronic indexing of the phased array, as illustrated in Figure 4) and adjust probe focus to accommodate the more complex structure of these panels. Data acquired with this method yields a 3-D volume of reflection data. The data are collected such that a single amplitude value is recorded for each point in the inspected 3-D volume. For the 16" x 16" panels used in this study, such single point data collection amounts to over 180 Mb of data per panel when data acquired with 1 mm lateral resolution at a 50 MHz data acquisition rate. However, because the acoustic impedance of the elastomeric material is dramatically different than that of the carbon-based matrix, very little of the incident acoustic energy is able to penetrate through this layer. Therefore, each panel was inspected twice, once from each side. Given the differences in properties and layout on either side of the elastomer, different inspection methodologies were used on either side.

In the general case for immersion scanning ultrasonic methods (be it phased array or single transducer), when the exact location/depth of a defect(s) is not known, a 2-D representation of the scanned data can be obtained in the form of a c-scan, or 2-D map of peak amplitude as a function of scan and index position across the face of the plate. Usually this C-scan information is produced by selecting the peak amplitude from the reflections within the material, independent of depth. To provide some depth information for that peak amplitude pulse, a time-of-flight (TOF) c-scan often accompanies an amplitude c-scan. The arrival time of that peak, for a *monolithic specimen*, is linearly correlated to the depth from which that peak amplitude was reflected. However, if the plane or depth of the defect is well known then only the reflected pulse data from that plane are of interest. In such a case, in the A-scan data, a "time-width gate" can be set and ONLY data from within that time window will be used for the resulting C-scan. The size of the digital data set in such a case becomes much more manageable. Examples of conventional C-scan results for one of the armor panels are shown in Figure 3 below, in which timing gates were set around the first, second and third reflections from the Matrix/Elastomer interface.

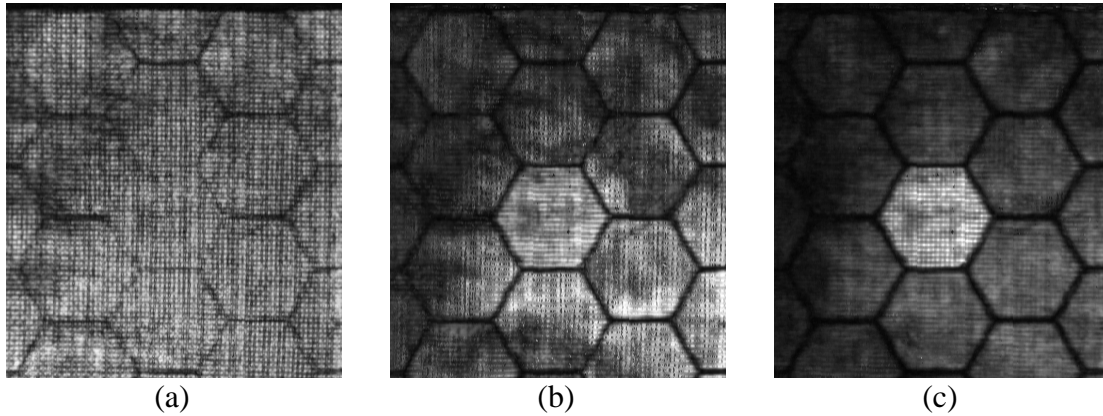


Figure 3. Conventional C-scan images of reflection from the Matrix/Elastomer boundary with timing gates centered on a) first, b) second and c) third reflections.

When the specimen to be studied by ultrasound is not monolithic, e.g., is a layered medium such as these composite armor samples, or if a sample contains a number of distinct closely “stacked” defects (i.e., multiple defects that occur along a line normal to the inspection surface) then the ultrasound process becomes more complicated. In such a case, the issue becomes a matter of trying to distinctly identify one layer separate from the others. In this case, the conventional C-scan approach, which is only able to capture information for a single location/depth for each point on the inspected surface, is often unable to specifically identify/locate a defect unless it happens to coincide with the most reflective interface, and is generally unable to distinguish between multiple collinear defects. Furthermore, when only a single plane is of interest, and the defect(s) of interest coincides with that plane, reflections from other interfaces in a layered medium may overlap that response, masking the effect of the defect. In these cases, the defect signature is often still present within the full data set, but extracting that signature using automated methods becomes a challenge. Insonification from the top surface of an armor panel generates multiple reflections, as demonstrated in Figure 4a. While the timing control afforded by the phased-array system naturally reduces the effect of interfaces near the surface, those close to the interface of interest are relatively in-phase with reflections from this interface, and thus can contribute significant noise. This is seen in Figure 4b in which the discrete reflections from the Matrix/Elastomer interface (the 6 narrow dark bands labeled R1 through R6) are interspersed with additional reflections from other interfaces (as indicated by the additional gray bands throughout the B-scan, especially in the top half). With regard to the issue of multiple layer reflections, the current effort has evaluated two filtering methodologies which significantly improve the signal-to-noise ratio over conventional methodologies. These filtering techniques have been applied to the received signals from ceramic-side inspections (where the multiple layers of high-velocity materials give rise to many interfering reflections), but are not of particular use for signals from support layer side inspections (where the tile is essentially monolithic down to the elastomer-matrix interface, and very little acoustic energy is reflected from interfaces beyond that one).

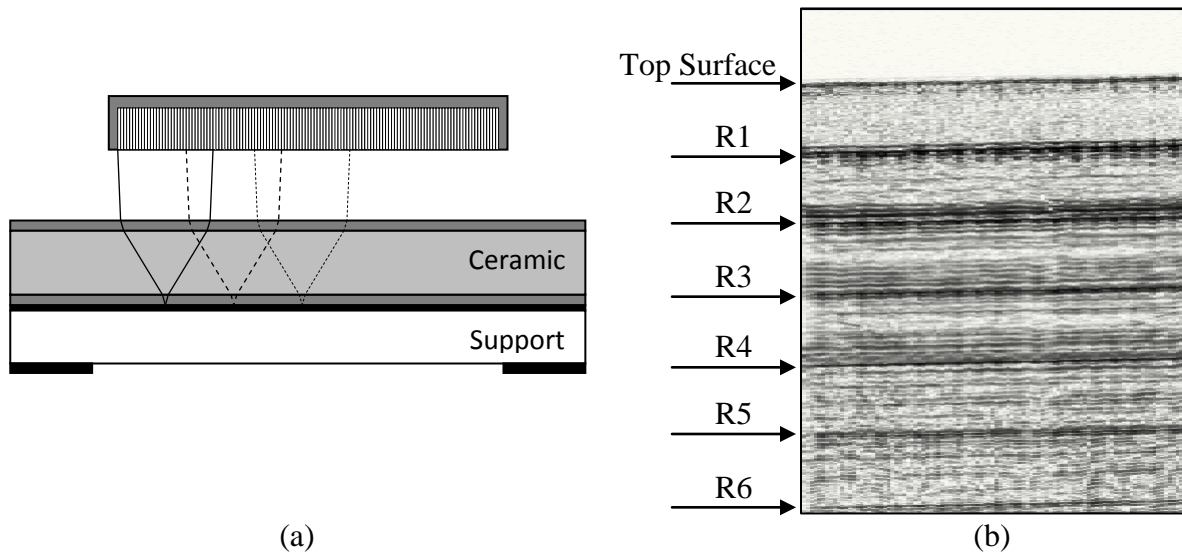


Figure 4. a) Schematic diagram of phased-array inspection of layered armor panel and b) resulting B-scan plotting reflected acoustic amplitude as a function of depth (vertical axis) and position on the panel (horizontal axis).

RESULTS

Graphite-side Inspection

FFT filtering: Each interface (Water/Matrix, Matrix/Ceramic, Ceramic/Matrix, Matrix/Elastomer, Elastomer/Support and Support/Water) will reflect a portion of the acoustic energy incident thereon. The relative amplitude of that reflection is dependent upon the acoustic impedance mismatch between the two materials forming that interface. Thus, while there will be reflections from all five interfaces, the reflections from the first (Water/Matrix, which reflects ~80% of the incident energy in this case) and fourth (Matrix/Elastomer, which reflects ~75% of the incident energy in this case) interfaces will have the largest amplitudes. Unfortunately, the propagation time between the first, Water/Matrix, and second, Matrix/Ceramic, reflections (as well as between the third Ceramic/Matrix and fourth, Matrix/Elastomer) will be fairly small (a fraction of a microsecond), given the relatively high velocity in the relatively thin matrix layers. Because the time duration of each reflected acoustic pulse is of the same order as the separation between the reflections from these interfaces, the reflections overlap in time. This is true of the first and second reflections from these interfaces (where the acoustic pulse is reflected between the subsurface interface, the surface of the tile, and the subsurface interface a second time). Not until the third and subsequent reflections from each of these interfaces are they sufficiently temporally separate as to be able to distinguish them (see the A-scan of Figure 5 below). However, the acoustic velocity is independent of amplitude and thus the temporal spacing between higher-order reflections is constant. Therefore, if we select only those components of the reflected acoustic signature that are periodic at this temporal spacing we should be able to greatly enhance the signal-to-noise ratio (SNR) for that interface. By examining the acoustic waveform in the frequency domain we can simply select only that frequency that corresponds to this temporal period (i.e., at the resonance frequency of the Matrix/Ceramic/Matrix “sandwich”), and the amplitude of that frequency component will be directly related to the reflectance of the

interface of interest. Using this amplitude allows plotting scans for all positions in the “FFT Filtered” -scans. An example for one such scan for panel D3 is shown in Figure 7a below. Interestingly, one additional benefit of this approach is the segregation of tile types. Because the two grades of tile used in these panels have different acoustic velocities, they also have different resonance frequencies. By selecting the frequency corresponding to the higher-performing tile material (with the higher acoustic velocity), only that tile type contributes significantly to the FFT-filtered C-scan of Figure 7. This is further illustrated in the B-scan of Figure 6a below which shows the different time/depth spacing of the two tile types (with the higher-performance tile in the center). One can then alternatively select the frequency corresponding to the alternate tile type to arrive at the FFT-filtered C-scan of Figure 6b, which not only emphasizes the alternate tile regions, but also reveals a C-shaped defect in the tile just above the center tile.

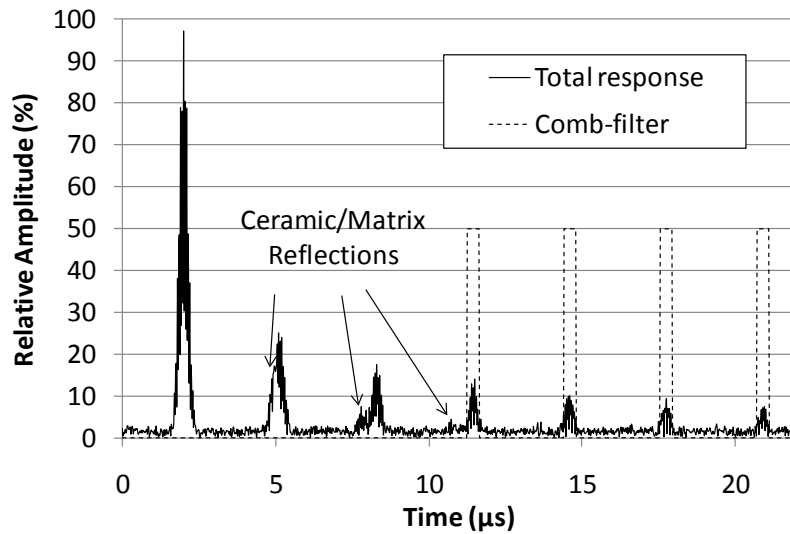


Figure 5. Schematic diagram of a theoretical A-scan showing reflections from interfaces within a multiple layered-structure. For clarity, the waveform shown includes only the components of the waveform due to the Ceramic/Matrix and the Matrix/Elastomer interfaces.

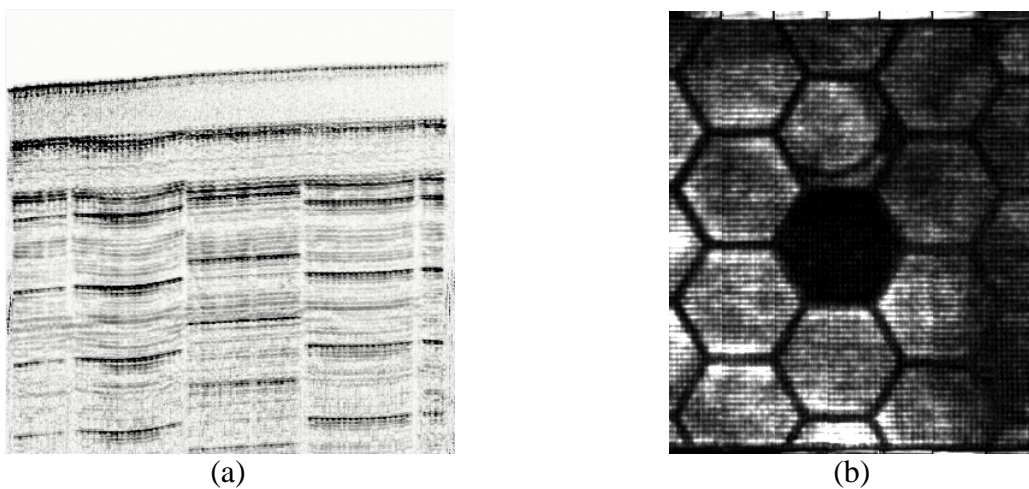


Figure 6. a) B-scan of Ceramic-side inspection showing the different resonances for different tile materials, b) FFT-filtered C-scan tuned to examine the lower-performance tile regions.

Comb filtering: While the FFT filtering has the advantages of being very straightforward (requiring only velocity and thickness information for each material used) and including all transits between the Water/Matrix and Matrix/Elastomer interfaces (including those initially generated by other reflections), it still includes the initial front-surface reflection and the “ring-down” from the first Ceramic/Matrix interface reflection in its analysis, and thus may not maximize the SNR (as these reflections do not contain any data about the interface in question). This is reflected in the slightly stronger weave pattern shown in the FFT results of Figure 7a (as compared with the Comb filter results of Figure 7b). A more direct approach was therefore attempted. This approach required one additional piece of information – the arrival time of the Water/Matrix interface front-surface reflection. Once that is known, the exact arrival times for all subsequent reflections can be determined (again – if the velocity and thickness information for each layer is known) in a “front-follow” arrangement. A “comb-filter” can then be constructed to pass only those components of the acoustic waveform that correspond to the arrival times of reflections from the interface of interest, beginning with the third (where temporal separation from other reflections begins). By integrating the response within each of these reflections, the comb-filtered waveform is able to distinguish the reflection from the interface of interest, thereby maximizing the phased—array reflection pulse sensitivity to defects at that interface, as shown in Figure 7b. However, it is worth noting that, while neither of these images reveal the included artificial “disbond” (as might be expected, given the already very high mismatch in impedance between the Matrix and Elastomer layers), there is clearly non-uniformity in the amount of acoustic energy reflected from this interface. The high-reflectivity regions on the interface are more clearly evident using the comb-filter technique, while the low-reflectivity regions are better visualized using the FFT method. Since we do not yet know which is a better predictor of ballistic performance, data was acquired for all samples using both techniques.

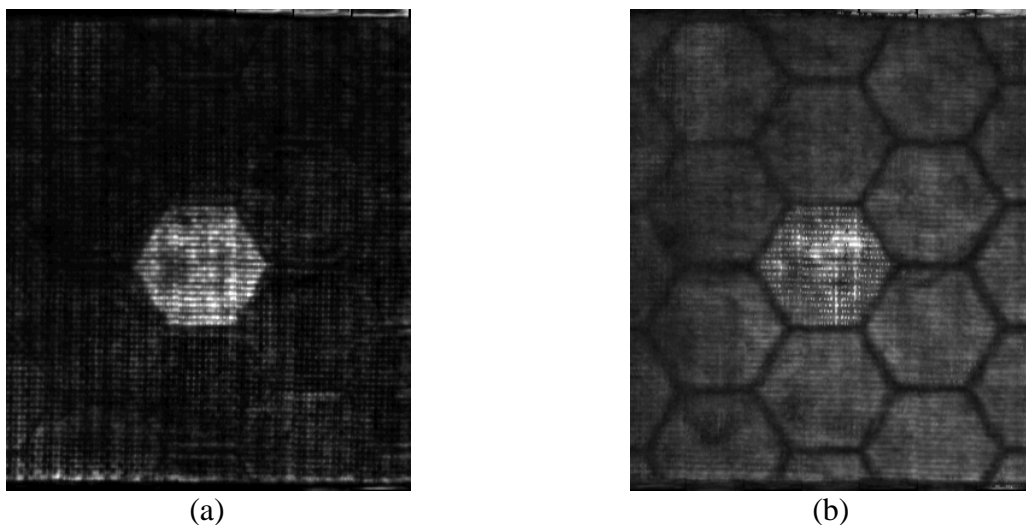


Figure 7. Phased array ultrasound data filtered c-scan data for tile D3, inspected from the graphite-side, using the a) FFT analytical method and b) comb-filter technique.

S2-side Inspection

Insonification of the armor tile from the Support side of the tile presents essentially a monolithic material, as the acoustic impedance of the Support and Elastomer materials are

virtually identical. A conventional c-scan approach, properly employed, can therefore be applied for inspection of the Support/Elastomer interface, as this interface will typically be the most reflective plane within the layered structure (as much of the acoustic energy incident on the Matrix side of the Elastomer will be totally internally reflected within the Elastomer). However, if there are any smaller defects present within the thickness of the Support layer a conventional c-scan approach will be insensitive to these defects. Thus, for our results from these inspections, two c-scan images are provided. The first is a conventional c-scan in which the phased array is focused on the Elastomer/Matrix interface for both transmission and reception. The second specifically excludes this interface from the resulting a-scans and examines the remainder of the volume of the Support and Elastomer materials for either additional discontinuities within the Support material, or degradation of the Support/Elastomer interface. In either case, any defect revealed can be further analyzed using the full data set. An example of this approach is shown in Figure 8 below. Figure 8a shows a B-scan (essentially a vertical slice through the 180 Mb data set) of the Support material in panel C5. The Support/Elastomer interface is barely distinguishable at a “depth” of approximately $13\ \mu\text{s}$ (given the virtually identical impedances for these two layers, less than 1% of the energy would be reflected from an intact interface). However, there is also a much more pronounced intermediate reflection at an apparent “depth” of approximately $11\ \mu\text{s}$ – within the Support material. For reference, the same cross-sectional “slice” from panel C6 is shown in Figure 8b. Here, the Support/Elastomer interface is not really visible at all at $13\ \mu\text{s}$, but there is no intermediate reflection at $11\ \mu\text{s}$. Instead, though a reflection is seen at approximately $5\ \mu\text{s}$. Figure 9a shows a c-scan of the Support and Elastomer material layers in panel C5, where a reduced reflection is clearly evident (in the form of a thumbprint-shaped region protruding from the lower left quadrant of the image), indicating that there is a higher reflection (i.e., a defect) covering the entire sample outside the thumbprint-shaped region. The TOF scan in Figure 9b shows that the peak amplitude within this thumbprint-shaped region is coming from near the Elastomer/Matrix interface, but that the peak signal in areas outside this region comes from within the Support material itself. This would therefore indicate that a “disbond” within the Support layer has occurred everywhere outside the thumbprint region. Thus, if detection and location of these non-interfacial defects are of interest, the inspection methodology must be able to maximize sensitivity to all possible depths within the Support material, not just the Support/Elastomer interface.

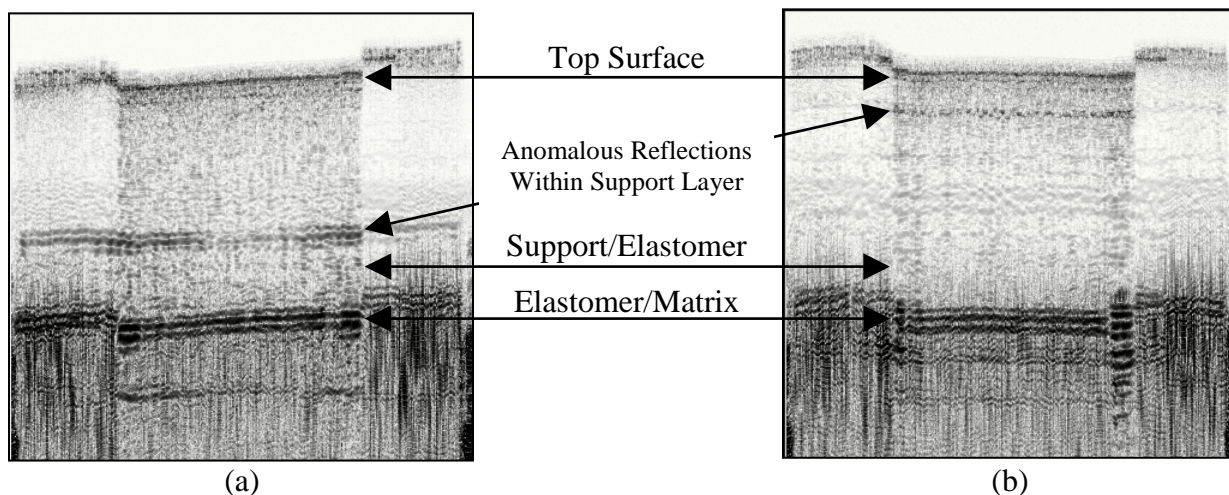


Figure 8. 10 MHz Phased array B-scan data for S2-side insonification of tiles a) C5 and b) C6.

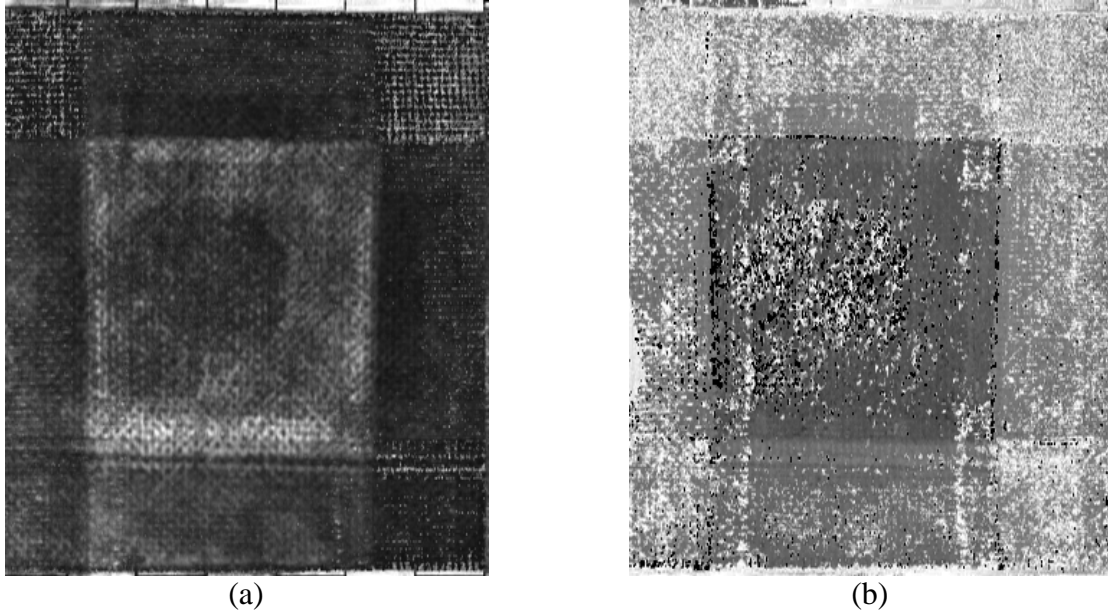


Figure 9. Phased array C-scan data for tile C5. a) Conventional C-scan of the Support and Elastomer, showing a thumbprint-shaped reduced reflection region, and b) TOF image, showing a uniform time/depth of $11\ \mu\text{s}$ below the surface for the area outside this region

In cases where an artificial “disbond” was introduced between the Support and Elastomer layers, one would expect to see a significant change in the reflected energy, as this defect would markedly alter the acoustic impedance mismatch of that interface. This is clearly seen in the B- and C-scans of panel J3, shown in Figure 10 below. The B-scan of Figure 10a was taken along a vertical line through the center of the panel, bisecting the $\frac{1}{2}$ ” square defect. Of note is the fact that, in addition to revealing the defect, the B-scan also indicates that the overall integrity of the Support/Elastomer interface is not as strong as was observed in the earlier panels of Figure 8.

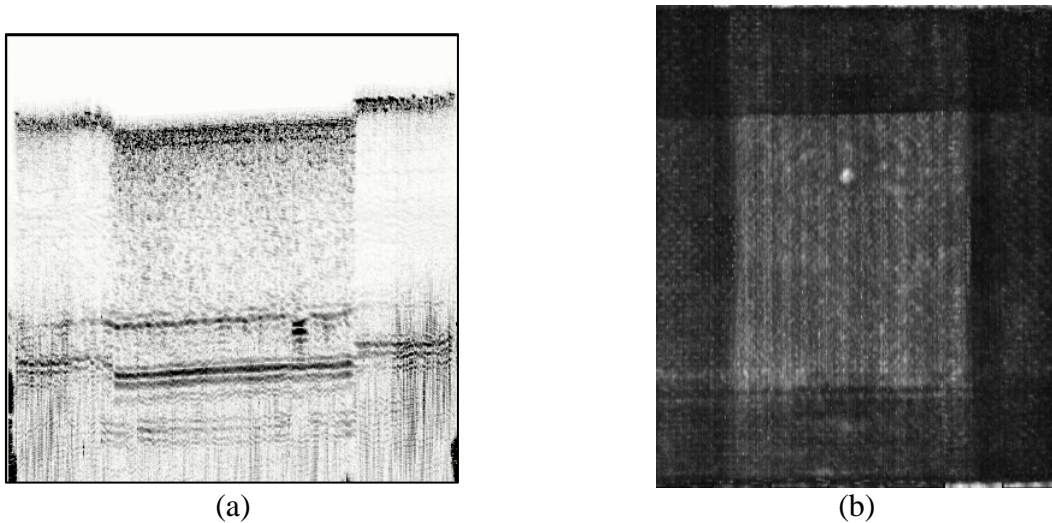


Figure 10. a) B-scan and b) C-scan of panel J3 clearly indicating the included defect within the Support/Elastomer interface.

CONCLUSION

In summary, two specific digital signal processing techniques have been developed to help improve phased array ultrasonic inspection and analysis of multi-layered ceramic armor panels. The location of some of the specific layered materials, especially the highly attenuative central Elastomer layer, suggests that ultrasonic inspections for locating and identifying internal defects be conducted from each side of the panels. In addition, because of the specific properties of the layers, different inspection methodologies should be used for each side in order to maximize detection sensitivity. Inspection from the Ceramic side, where the multiple layers of high-velocity materials create multiple and often overlapping acoustic reflections, use of an FFT or Comb-filtering technique likely would be best to locate and identify interfacial defects. The detection sensitivity from these two methods differs slightly. Comparing these two techniques to determine which of the two is the “better” method depends upon the predictability of ballistic performance provided by each technique.

Unlike the Ceramic-sideinsonification, where multiple high-velocity layers are present, inspection from the Support side, in which the panel behaves largely as a monolithic material, can be accomplished without the additional signal processing. Detection of interfacial defects at the Support/Elastomer interface has been clearly demonstrated. However, in cases where defects occur within the Support layer (a particularly likely scenario for post-impact examination, but still observed even within the untested panels), it is critical not only that these defects be detected (even when multiple “stacked” defects are present) but that the sensitivity of the detecting system be maximized for that detection. This would best be performed using the Dynamic Depth Focusing (DDF) method unique to phased-array inspection. In this method, the acoustic energy is transmitted into the material with a time delay between array elements that will “focus” the energy at a particular depth (say, the Support/Elastomer interface). If only interfacial defects are of interest, a simple c-scan of the reflection from this interface is sufficient to identify and locate those defects. However, if defects within the bulk of the Support material are also of interest (as is clearly the case for the panels presented here, in which there appears to be some kind of planar defect within the Support layer), DDF allows for the time delay between array elements to be adjusted dynamically so that the *received* signals are “focused” at each reflecting depth rather than the transmitted depth only (as would be the limitation for conventional ultrasound). This greatly enhances both the sensitivity to and fidelity of non-interfacial defects without compromising sensitivity to interfacial defects, and thus will be the focus of our continuing efforts, particularly as we examine the panels after ballistic impact.

REFERENCES

- ¹ J.M. Wells, W.H. Green and N. L. Rupert—“On the Visualization of Impact Damage in Armor Ceramics”, *Eng. Sci. and Eng. Proc.*, **22** (3), H.T. Lin and M. Singh, eds, pp. 221-230 (2002).
- ² J. S. Steckenrider, W. A. Ellingson, and J. M. Wheeler “Ultrasonic Techniques for Evaluation of SiC Armor Tile,” in *Ceram. Eng. and Sci. Proc.*, **26** (7), pp. 215-222 (2005).
- ³ R. Brennan, R. Haber, D. Niesz, and J. McCauley “Non-Destructive Evaluation (NDE) of Ceramic Armor Testing,” in *Ceram. Eng. and Sci. Proc.*, **26** (7), pp. 231-238 (2005).
- ⁴ G.P. Singh and J. W. Davies, “Multiple Transducer Ultrasonic Techniques: Phased Arrays” In *Nondestructive Testing Handbook*, 2nd Ed., **7**, pp. 284-297 (1991).

⁵ J. Scott Steckenrider, William A. Ellingson, Rachel Lipanovich, Jeffrey Wheeler, Chris Deemer, "Evaluation of SiC Armor Tile Using Ultrasonic Techniques," *Ceram. Eng. and Sci. Proc.*, **27** (7), (2006).

⁶ D. Lines, J. Skramstad, and R. Smith, "Rapid, Low-Cost, Full-Wave Form Mapping and Analysis with Ultrasonic Arrays", in Proc. 16th World Conference on Nondestructive Testing, September, 2004.

⁷ J. Poguët and P. Ciorau, "Reproducibility and Reliability of NDT Phased Array Probes", in Proc. 16th World Conference on Nondestructive Testing, September, 2004.